Scalability of mass transfer in Taylor flow in capillaries

Valentina NAPPO, Simon KUHN*

* Corresponding author: Email: simon.kuhn@ucl.ac.uk
Department of Chemical Engineering, University College London, UK

Abstract In the present work, gas–liquid hydrodynamics and mass transfer in horizontal circular capillaries of different diameters are investigated experimentally. The capillary diameters range from 0.5 to 3.2 mm in order to investigate the mass transfer process on both micro and milli scale. The mass transfer is studied using the chemical absorption of CO_2 into an alkaline solution. A high speed camera is used to capture images of the flow. Subsequently, the images are analysed thought a specifically developed Matlab code. Such a code is able to extract important hydrodynamic parameters (bubble length, liquid slug length, void fraction, film thickness, bubble velocity etc.) that affect the mass transfer coefficient, k_La. The obtained results both for the hydrodynamics of the flow and for the mass transfer are compared with those present in literature, and the scalability of the mass transfer coefficient is assessed.

Keywords: Taylor Flow, Mass transfer, Capillary, Two phase flow, Scale up.

1. Introduction

During the last decades gas–liquid two–phase flow in microchannels has attracted considerable attention [1][2][3] thanks to the numerous advantages that the microscale devices present over the conventional systems [4]. The decrease in size of the reactors, in fact, results in a very high surface to volume ratio that is particularly beneficial for increasing heat and mass transfer. In addition these devices provide a very low pressure drop. The main drawback of micro-reactors is their inadequate throughput for industrial applications. For this reason scale-up of these systems is necessary. In this light, a detailed study on the mass transfer on different scales is the first step to achieve this objective.

The typical regimes that may occur in micro–structured reactors are: bubbly flow, Taylor flow, slug-bubbly flow, churn flow and annular flow. Over the last decades researchers have focused on Taylor flow regime because of its superior mass transfer performance [5]. Figure 1 depicts a schematic representation of Taylor flow. It consists of an alternating sequence of gas bubbles and liquid slugs. The length of the gas bubbles is larger than the channel diameter and a thin liquid film separates the gas bubbles from the channel walls. In contrast to the single phase regime, in Taylor flow the formation of two vortexes can be observed within the liquid slug [6]. The recirculation caused by the vortexes enhances the radial mixing and, consequently, the heat and mass transfer in the radial direction [7] [8]. On the other side, the characteristic segmented flow reduces the axial mixing [9].

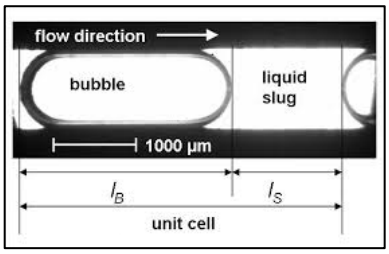

Figure 1 Schematic of Taylor flow [10] .

Several correlations have been developed in order to predict mass transfer. Berčič and Pintar [11] proposed a correlation for the mass transfer coefficient, k_La, for methane absorption into water in a glass capillary and they found that the mass transfer coefficient mainly depends on the slug liquid length and two–phase velocity (U_G+U_L) (eq.1).

$$k_L a = 0.111 \frac{(U_G+U_L)^{1.19}}{[(1-\varepsilon_G)\cdot L_{UC}]^{0.57}} \quad (1)$$

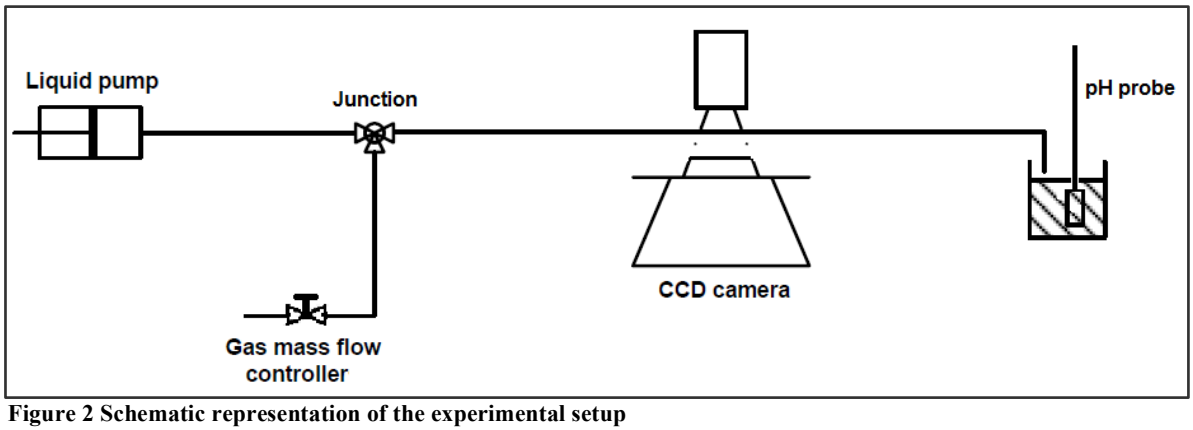

Figure 2 Schematic representation of the experimental setup

Where k_La denotes the mass transfer coefficient, U_G and U_L are the gas and liquid superficial velocities, respectively, ε_G is the gas hold-up, and L_{UC} is the unit cell length.
It is worth noticing that this equation has been obtained for relatively large bubble lengths and could not be applicable for different fluid systems. Van Baten and Krishna [8], instead, theorized that it is possible to divide the mass transfer in two contributions, one due to the liquid film and the other due to the bubble cap. Therefore, in their computational fluid dynamic study they proposed a correlation that accounts separately for these two effects (eq.2).

$$k_La = k_{L,cap}a_{cap} + k_{L,film}a_{film} = \\ = \frac{2\sqrt{2}}{\pi}\sqrt{\frac{\mathcal{D}\cdot U_G}{d_c}}\cdot\frac{4}{L_{UC}} + \frac{2}{\sqrt{\pi}}\cdot\sqrt{\frac{\mathcal{D}\cdot U_B}{\varepsilon_G\cdot L_{UC}}}\cdot\frac{4\cdot\varepsilon_G}{d_c} \qquad (2)$$

Where $\mathcal{D}$ denotes the diffusivity, d_C is the capillary diameter, and U_B is the bubble velocity.
Later, Vandu et al. [12] suggested a correlation based on the $k_{L,film}a_{film}$ proposed by Van Baten and Krishna. Their correlation is valid for relatively short unit cells (eq. 3).

$$k_La = C_1\sqrt{\frac{\mathcal{D}\cdot U_G}{L_{UC}}}\cdot\frac{1}{d_c} \qquad (3)$$

Where C_1 is a constant. For air absorption in water a value of 4.5 for C_1 was found as the best to fit the experimental data [12].
Finally, Yue et al. [13] developed a correlation (eq.4) based on non–dimensional numbers (Reynolds, Sherwood and Schmidt numbers).

$$Sh_L\cdot a\cdot d_c = 0.084\cdot Re_G^{0.213}\cdot Re_L^{0.937}\cdot Sc_L^{0.5} \qquad (4)$$

This approach is particularly advantageous as it allows us to estimate the mass transfer coefficient from superficial velocities and fluid properties, and does not rely on the knowledge of local quantities, such as bubble or slug lengths. However, this correlation completely ignores the flow pattern characteristics inside the channel. This can results in an inaccurate estimation of k_La.

2. Experimental

2.1 Reaction system

In this work a chemical absorption of CO_2 into an alkaline solution (NaOH) is taken into account. This reaction is particularly suitable as it occurs in the absence of a catalyst, and the conversion of the reactants can be monitored through the value of pH. In addition, it is an industrially relevant reaction as it is used for the CO_2 removal from the syngas for ammonia [14], CO_2 removal from the flue gas [15], and other environmental [16] and medical [17] [18] applications.
The chemical absorption of CO_2 into an alkaline solution follows the steps [19]:

$$CO_{2(G)} \leftrightarrow CO_{2(L)} \qquad (i)$$

$$CO_{2(L)} + OH^- \leftrightarrow HCO_3^- \qquad (ii)$$

$$HCO_3^- + OH^- \leftrightarrow CO_3^{2-} + H_2O \qquad (iii)$$

So the overall reaction can be written as:

$$CO_{2(L)} + 2OH^- \leftrightarrow {CO_3}^{2-} + H_2O$$

The first step represents the physical dissolution of CO_2 into the water. The rate of this process is comparatively high so it can be assumed that equilibrium conditions are reached at the interface. In addition, the rate of the last step is significantly higher than the first one. Therefore it can be assumed that reaction (ii) governs the rate of the process.

2.2 Experimental setup

Fig.1 shows a schematic representation of the experimental setup. It mainly consists of a capillary, an images recording system, and a feed system for the fluids. The gas flow rate is precisely controlled through the use of a mass flow controller (MFC, Bronkhorst F–200CV with a range 0.1–5ml/min) while for the liquid a syringe pump (0–80ml/min) is used. The liquid phase consists of a NaOH solution (starting pH of 11) while the gas phase is CO_2. The fluids are fed to a horizontally mounted capillary through a T–junction. In addition back pressure regulators (20 psi) are used to stabilize the pressure in the system and to achieve a stable flux in the capillary. The first back pressure regulator is placed between the MFC and the T–junction, while the other is located between the syringe pump and the T–junction. Three different circular capillary diameters (0.5 mm, 1.55 mm and 3.2 mm) are used in the experiments. The range of capillary diameters is chosen in order to investigate system hydrodynamics and transport mechanisms on both micro- and milli-scale. Although there is no unique criterion to distinguish between micro and milli channels, it can be generally assumed that if the interfacial forces dominate over gravity then the channel can be classified as a micro-scale system [20]. A method based on this approach, consists of the calculation of the Laplace constant, defined as follows:

$$\lambda = \sqrt{\frac{\sigma}{g\cdot(\rho_L - \rho_G)}} \qquad (5)$$

where σ denoted the interfacial tension of the fluid system, g the gravitational acceleration and ρ the densities of each phase. If the diameter is smaller than the Laplace constant then the influence of the gravity on the system is negligible in comparison to that of the interfacial forces, and the channel can be considered a micro-channel. For the present system the calculated Laplace constant is 2.7 mm so the 0.5 and 1.55 mm capillaries can be classified as micro–systems, while the 3.2 mm capillary is on the milli–scale. All the experiments are conducted at room temperature and ambient pressure.

Upon exiting the capillary the two–phase mixture is collected in an open phase separator where the pH is measured via a pHmeter (Mettler Toledo) in order to evaluate the mass transfer coefficient, k_La. We are able to quantify the local mass transfer coefficient k_La according to

$$k_L a = \frac{j_L}{L} \ln\left(\frac{c^{eq} - c^{in}_{CO_2}}{c^{eq} - c^{out}_{CO_2}}\right), \qquad (6)$$

where j_L denotes the superficial liquid velocity, L the position in the reactor, c^{eq} the equilibrium concentration, $c^{in}_{CO_2}$ the CO_2 concentration at the inlet (which is zero for our conditions), and $c^{out}_{CO_2}$ the CO_2 concentration at the measurement location. It is worth noticing that, for our experimental system, CO_2 is chemically absorbed into the liquid, so there is no risk that it escapes from the alkaline solution before the measurement. For this reason there is no need to use a sealed phase separator.

Once a steady flow is achieved (2 – 3 min after the start of the flow), images of the flow pattern are recorded using of a Photron FASTCAM MC–1, while a cold lamp is used to provide the background illumination for the microchannel. The camera can be set to capture up to 2000 frames per second at maximum resolution (512x512). The images are analysed using a customized Matlab code. The code is responsible for the conversion of the images from grey scale to black and white and for providing important information about the flow pattern. After the binarization the code is able to distinguish between the

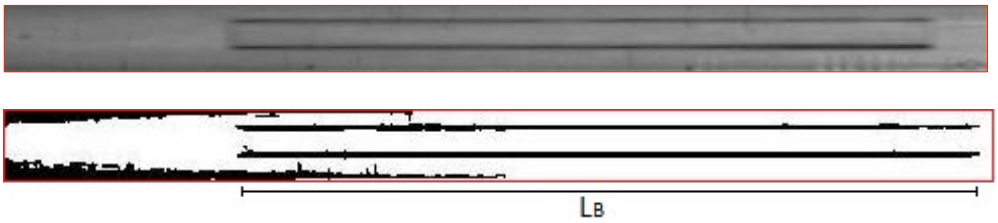

Figure 2 Image of gas–liquid flow inside the 0.5 mm capillary captured with the high speed camera before and after the binarization.

continuous and the dispersed phase and to measure parameters such as bubble and liquid slug length etc.

Figs. 2 and 3 show an image of the two–phase flow before and after the binarization. It can be seen that the developed code is effective for the post–treatment of the images and for the extraction of the flow pattern characteristics as it can clearly identify the bubbles inside the channel.

In addition, if the frame speed is significantly high (about 200 frames per second) then it is possible to have sequential images of the same bubble travelling along the microchannel. This enables to measure the bubble velocity and, so, to estimate the gas void fraction and the slip ratio.

The bubble velocity, in particular, is determined by measuring the time required for the gas bubble to travel over a known distance in the capillary and it is an average of about 5 values. The two-phase void fraction is defined as:

$$\varepsilon_G = \frac{V_G}{V_G+V_L} \tag{7}$$

where V_G denotes the volume occupied by the gas and V_L the volume occupied by the liquid phase inside the channel. As Taylor flow is classified as a non-homogeneous flow, the void fraction cannot be deducted from the inlet fluxes, i.e. it cannot be considered equal to the gas volume transport fraction, defined as:

$$\dot{\varepsilon}_G = \frac{\dot{Q}_G}{\dot{Q}_G+\dot{Q}_L} \tag{8}$$

where $\dot{Q}_G$ represents the gas volume flow rate and $\dot{Q}_L$ the liquid volume flow rate.

These parameters are related through the slip ratio:

$$S = \frac{v_b}{v_L} = \frac{\dot{\varepsilon}_G(1-\varepsilon_G)}{\varepsilon_G(1-\dot{\varepsilon}_G)} \tag{9}$$

For homogeneous flow patterns, S is equal to one, while for Taylor flow values higher than unity are observed. As we are dealing with two-phase flows in capillaries it is very difficult to accurately measure the diameter of the bubbles through image analysis, due refraction induced by the wall curvature. In general, the bubble diameter extracted from image analysis is underestimated, and consequently also the total gas volume inside the capillary results in lower values. Therefore it is preferable to calculate the void fraction based on the bubble velocity measurements.

3 Results and discussion

Fig. 4 shows the effect of the gas volume transport fraction, $\dot{\varepsilon}_G$, on the bubble length for different capillary diameters. It can be seen that the bubble length gradually increases with $\dot{\varepsilon}_G$. In particular, an increase of $\dot{\varepsilon}_G$ has two effects: on one hand, it results in a higher quantity of gas injected into the capillary that tends to enlarge the bubbles, and, on the other hand, it causes an increase of the detaching effect that tends to shorten the bubble. As these phenomena work against each other, the increase in the bubble length shown into the graph means the gas injection dominates over the detaching effect in the selected range of gas and liquid flow rate.

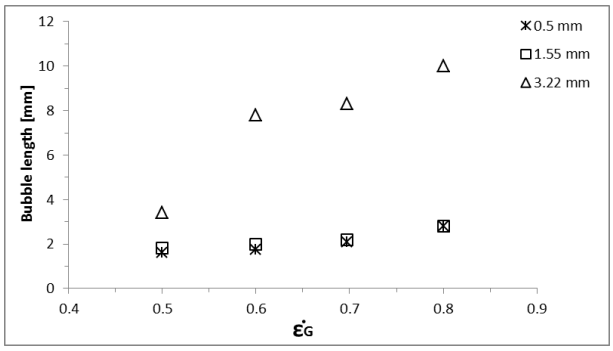

Figure 4 Effect of gas transport fraction on bubble length for three different capillary diameters.

Fig. 5 presents the variation of unit cell length, L_{UC}, as function of $\dot{\varepsilon}_G$. Also in this case the graph shows a gradual increase of this parameter as $\dot{\varepsilon}_G$ is increased. For the 3.22 mm capillary at $\dot{\varepsilon}_G$ = 0.5 both L_{UC} and the bubble length seem to be very low and deviate from the trend of the rest of data. This is probably due to a not completely stable flow when the images were recorded. For this reason a further analysis is necessary for this setup.

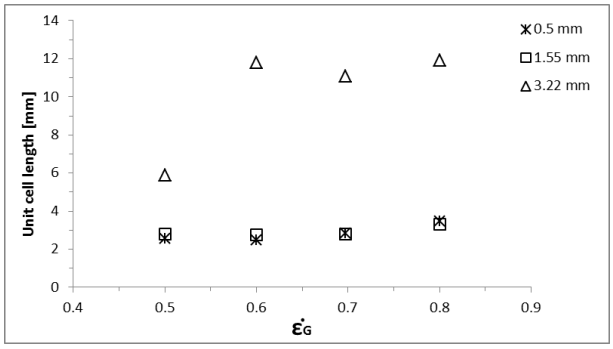

Figure 5 Effect of gas transport fraction on unit cell length for three different capillary diameters.

In addition, Figs. 6, 7 and 8 highlight the effect of the increase of the two-phase flow velocity, U_{TP}, at fixed $\dot{\varepsilon}_G$. It is shown that an increase in U_{TP} results in a decrease of both gas and liquid slug length for $\dot{\varepsilon}_G$ = 0.5 (Fig 6). This phenomenon is probably due to the increase of the liquid drag force which causes the formation of shorter bubbles. For d_c=3.22 mm, obviously, the same anomaly is present. For $\dot{\varepsilon}_G$=0.7 two sets of data are presented in Figs. 7 and 8. It is worth noticing that, for the 3.22 mm capillary, the bubbles length increases with increasing U_{TP}, in contrast to the smaller capillaries data. It can be hypothesized that, for the largest capillary, the increase in the liquid drag force does not affect the bubbles formation process for the selected range of gas and liquid flow rate.

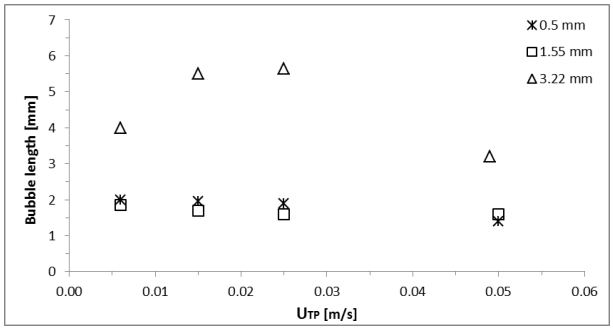

Figure 6 Effect of two phase velocity (U_G + U_L) on bubble length for three different capillary diameters at fixed $\dot{\varepsilon}_G$ = 0.5.

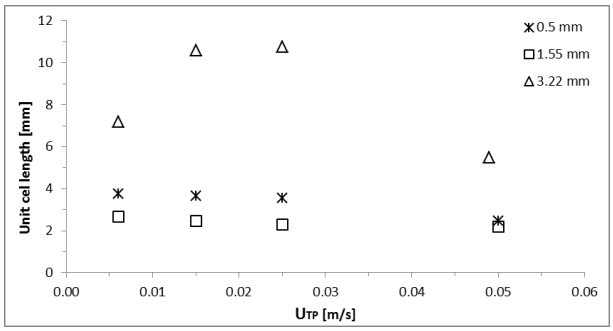

Figure 7 Effect of two phase velocity (U_G + U_L) on unit cell length for three different capillary diameters at fixed $\dot{\varepsilon}_G$ = 0.7.

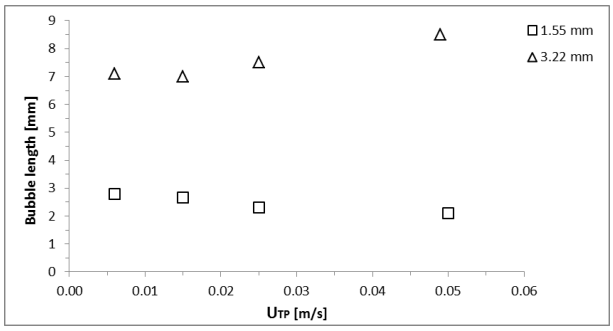

Figure 8 Effect of two phase velocity (U_G + U_L) on bubble length for two different capillary diameters at fixed $\dot{\varepsilon}_G$ = 0.7.

4 Conclusion and perspectives

In this work gas–liquid two–phase flow has been investigated in three circular capillaries with different diameters. On the base of Laplace theory, the largest capillary (3.22 mm) has been classified as a milli–channel while the others (1.55 and 0.5 mm) as micro–channels. Therefore, the selected system results suitable for the study of scalability of mass transfer in capillaries.
It was found that an increase of the gas volume

transport fraction, ε_G, or the two–phase velocity, U_{TP}, results in increased bubble length and decreased slug length. However the effect on the slug dimensions seems to be less significant than that on the bubbles as the unit cell length was also found to be increased with the increase of ε_G or U_{TP}. In addition, an increase in two phase velocity showed a decrease in bubble length for 0.50 mm and 1.55 mm capillaries, while, an increase was found for the 3.22 mm capillary at ε_G=0.7.

The next steps of this study will be carrying out further investigations in order to get a detailed knowledge of the hydrodynamics of the system. The investigation will be based on the described optical techniques (high speed camera) coupled with a customized Matlab code for the post–treatment of the images. The collected data describing the flow pattern will be used to model the mass transfer in the capillaries for both the micro and the milli–scale. In addition the mass transfer coefficient will be evaluated through the experiments using eq.6 and the results will be compared with those present in literature. The obtained results will contribute to quantifying the effect of two-phase flow hydrodynamics at each scale on the mass transfer coefficients and their scalability across several orders of length scale.

References

[1] Assmann, N., Ladosz, A., Rohr, P. R. (2013) *Chem. Eng. Technol.*, 36: 921–936
[2] Hassan, I., Vaillancourt, M., Pehlivan, M., (2005). *Microscale Thermophys. Eng.* 9: 165-182.
[3] Triplett, K.A., Ghiaasiaan, S.M., Abdel-Khalik, S.I., Sadowski, D.L., (1999). *Int. J. Multiphase Flow* 25: 377-394.
[4] Ehrfeld, Hessel, Loewe, (2000). Wiley-VCH, Weinheim, Germany.
[5] Liu, H., Vandu, C.O., Krishna, R., (2005). *Ind. Eng. Chem. Res.*, 44: 4884-4897.
[6] Thulasidas, T. C.; Abraham, M. A.; Cerro, R. L. *Chem. Eng. Sci*. 1997, 52, 2947-2962.
[7] Irandoust, S.; Andersson, B, (1989). C*omputers Chem. Eng.* 13: 519-526.
[8] Baten, J.M., Krishna, R., (2004). *Chem. Eng. Sci*. 59: 2535-2545.
[9] Salman, Gavriilidis, (2005). *Chem. Eng. Sci.* 60(22): 5895-5916.
[10] Völkel, N., Widianto, A. Y., Aubin, J., Xuereb, C. (2008). Gas-Liquid Taylor Flow Characteristics in Straight and Meandering Rectangular Microchannels, in 10th *IMRET*, April 6-10, 2008, New Orleans.
[11] Berčič, G., Pintar, A., (1997). *Chem. Eng. Sci.* 52: 3709–3719.
[12] Vandu, C.O., Liu, H., Krishna, R., (2005). *Chem. Eng. Process.* 60: 6430–6437.
[13] Yue, J., Chen, G., Yuan, Q., Luo, L. Gonthier, Y., (2007). *Chem. Eng. Sci.* 62: 2096–2108.
[14] Farrauto, R. J.; Bartholomew, C. H., (1997). Blackie Academic & Professional: London.
[15] Freguia, S.; Rochelle, G. T., (2003). *AIChEJ*, 49: 1676-1686.
[16] Aroonwilas, A., Veawab, A., Tontiwachwuthikul, P. (1999). *Ind. Eng. Chem. Res.*, 38: 2044 – 2050.
[17] Knolle, E., Heinze, G., Gilly, H. (2002). *Anesth. Analog.* 95:650–655.
[18] Knolle, E., Heinze, G., Gilly, H. (2003). *Anesth. Analog.* 97:151–155.
[19] Danckwerts (1993), *Chem. Eng. Sci.*, 48: 153-158.
[20] Serizawa A.; Feng Z.; Kawara Z., (2002). *Experimental Thermal and Fluid Science* 26: 703–714.